JOURNAL OF GEOPHYSICAL RESEARCH, VOL. 107, NO. B12, 2347, doi:10.1029/2001JB000401, 2002

Three-dimensional inversion of marine magnetic anomalies on the equatorial Atlantic Ridge (St. Paul Fracture Zone): Delayed magnetization in a magmatically starved spreading center?

Bertrand Sichler and Roger Hékinian

Institut Français de Recherche pour l'Exploitation de la Mer, Brest, France

Received 25 April 2000; revised 24 March 2002; accepted 29 March 2002; published 14 December 2002.

[1] The St. Paul Fracture Zone (FZ) in the equatorial Atlantic is interrupted by three intratransform ridge (ITR) spreading centers. A detailed magnetic survey, corrected for the diurnal variations using a moored magnetic station, six submersible dives, and three bottom-towed video camera tracks provide data on the most eastern ITR (0°37′N, 25°27′W). Visual observations and submersible sampling displayed a high ultramafic/volcanic ratio, supporting the assumption that the ITR is in a magmatically starved state. Volcanics were mainly found on the rift valley floor from 4700 to 4000 m and as a thin cap (<160 m) on the top of the eastern rift crest (2700 m). Most of the rift walls consist essentially of serpentinized peridotites and gabbros. The magnetic data show a well-defined ridge centered anomaly. A generalized inversion method was applied to the field data to calculate the crustal equivalent magnetization, assuming that the seafloor is broken down into elementary cells of $1 \times 1 \times 0.5$ km^3 which fit the topography. The average of absolute value of equivalent magnetization is 2.7 A m^{-1}. The width of the central normal polarity (Brunhes epoch) is wider (at least 34 km) than that indicated by the NUVEL-1 kinematic model (24.5 km). This 40% excess is believed to be significant and is thought to be the result of prolonged chemical remanent magnetization acquired during the serpentinization of peridotites. In a magmatically starved accretion segment, we suggest that peridotites could continue to acquire magnetization as long as tectonic activities facilitate the circulation of seawater in the upper mantle. *INDEX TERMS:* 1517 Geomagnetism and Paleomagnetism: Magnetic anomaly modeling; 3260 Mathematical Geophysics: Inverse theory; 3035 Marine Geology and Geophysics: Midocean ridge processes; 3040 Marine Geology and Geophysics: Plate tectonics (8150, 8155, 8157, 8158); 3660 Mineralogy and Petrology: Metamorphic petrology; *KEYWORDS:* magnetic anomaly, equatorial Atlantic, stochastic inversion

Citation: Sichler, B., and R. Hékinian, Three-dimensional inversion of marine magnetic anomalies on the equatorial Atlantic Ridge (St. Paul Fracture Zone): Delayed magnetization in a magmatically starved spreading center?, *J. Geophys. Res.*, *107*(B12), 2347, doi:10.1029/2001JB000401, 2002.

1. Introduction

[2] Magnetic lineations in the oceans are the main evidence for seafloor spreading and plate tectonic models [*Vine and Matthews*, 1963]. The key idea of these authors was to associate the acquisition of the magnetization with the emplacement and cooling of oceanic crust. This theory implicitly implies that both phenomena are almost simultaneous since magmatic cooling is fast. The success of the theory shows that the simultaneity is certainly true for the extrusives (layer 2b). For example, on the southern Juan de Fuca Ridge [*Tivey*, 1994], it was shown that the seismic 2a layer corresponds to the magnetic layer. For the dike complexes (layer 2a) this simultaneity is more doubtful. On the Blanco Scarp, the extrusives are found to be 10 times more magnetized than the dike complex [*Tivey*, 1996].

0148-0227/02/2001JB000401$09.00

The contribution of deeper crustal layers to the magnetic anomalies has been debated for a long time [*Opdyke and Hékinian*, 1972; see also *Harrison*, 1987]. The efficient remanent magnetization of deeper layers could have been delayed during their thermochemical history. Ocean Drilling Program (ODP) results from holes 504B [*Kinoshita et al.*, 1989; *Pariso and Johnson*, 1989; *Pariso et al.*, 1995; *Smith and Banerjee*, 1986; *Stokking et al.*, 1996; *Hall and Muzzatti*, 1999], 735B [*Pariso and Johnson*, 1993], and 896A [*Stokking et al.*, 1996] have been used to lend support to the concept of the contribution of deeper crustal source layers to surface anomalies.

[3] Concerning the serpentinized peridotites as a possible source to the surface anomalies, this is still a questionable topic. Some magnetic studies on samples extracted from the ODP holes 670 and 920 both located near the Mid-Atlantic Ridge (age <1 Ma), show that the magnetic properties of similarly serpentinized peridotites can vary significantly [*Oufi*, 2000]. For instance, those from the site 920 carry a

strong remanent magnetization (mean natural remanent magnetizaiton (NRM) of 11.8 A m^{-1} and Koenigsberger's ration $Q = 4.9 \pm 1.8$) [*Lawrence et al.*, 1997] comparable to many oceanic basalts of the same age [*Johnson and Pariso*, 1993], and those from the site 670 carry softer magnetic properties (NRM $\approx$ 4 A m^{-1} and much smaller Q than that of oceanic basalts) [*Hamano et al.*, 1990]. The peridotites of the holes 895D and 895E, close to the Hess Deep (equatorial latitude) formed at a typical fast spreading center, are serpentinized at 70% or more: They display a stable NRM of 3.2 and 1.2 A m^{-1} (median values for dunites and harzburgites, respectively) and a median value of K' ratio $\approx$ 2.4 [*Kelso et al.*, 1996]. Other studies of oceanic peridotites display similar magnetic properties [e.g., *Dunlop and Prevot*, 1982]. As pointed out by the above authors, this means that many oceanic serpentinized peridotites may be a potential contributor to the surface anomalies, but their magnetic properties are more variable than that of oceanic basalts probably as a consequence of their magnetization acquisition mechanism.

[4] In the St. Paul's magmatically starved ridge segment with small amounts of volcanics, we will show that the peridotitic mantle is mainly responsible for the observed magnetic anomalies. The present work deals primarily with magnetic data obtained from the surface ship *Le Nadir* during the St. Paul cruise (January 1998) (Figures 1a, 1b and 1c, and Figures 2a, 2b, 2c, and 2d) and helped to confirm the magmatically starved state of the studied area (Figures 3a, 3b, and 3c). In addition to the magnetic survey, seafloor geological observations carried out during submersible dives and deep-towed camera stations helped to confirm the magmatically starved state of the studied area. At first glance, the magnetic anomaly (Figure 1c) displays a negative well-defined elliptic shaped zone, symmetrically located over the axial valley and its neighboring structures. This simple observation means that magnetic surveys over short north-south structures at equatorial latitudes are feasible and useful. Moreover, at these latitudes, the negative magnetic anomaly observed over the axis is indicative of a normal polarity magnetized block (see Appendix A) and represents the axial "Vine-Matthews-type" anomaly. The width of the negative anomaly perpendicular to the strike of axial valley, before the removal of the regional trend, is more than 46 km (Figure 1c and Figures 2a, 2b, and 2c at 47, 50, and 42 km, respectively). After the regional trend correction which balances the positive and negative anomalies, the width of the negative anomaly is still ~39 km (39, 41, and 37 km on the lines A, B, C, respectively, on Figure 4a). On the basis of the NUVEL-1 kinematic model [*DeMets et al.*, 1990] and the age of the Brunhes-Matuyama transition, 780 ka [*Cande and Kent*, 1995], the width expected for the Brunhes anomaly at this latitude is 24.5 km. In fact, the weak inclination of the field and the shortness of the magnetic structures distort the usual shapes of the magnetic anomalies. Hence we have to determinate the seafloor magnetization itself.

[5] In order to explain such an indicative discrepancy between measured width and expected width, a detailed magnetic study taking into account the seafloor topography, the short length of the axial accreting segment and the direction of the magnetic field is justified. In this paper, we investigate the distribution of the crustal equivalent magnetization with a three-dimensional (3-D) inversion of the magnetic data based on a generalized inverse method [*Tarantola and Valette*, 1982; *Menke*, 1984; *Tarantola*, 1987] (see Appendix A).

2. Geological Setting

[6] The two largest fracture zones (FZ) in the Atlantic, the Romanche and St. Paul FZs are both found close together near the equator (Figures 1a and 1b). The St. Paul's FZ located between 1°N–30°20′W and 0°30′N–24°W, offsets the Mid-Atlantic Ridge (MAR) by ~700 km. The satellite gravity data [*Sandwell and Smith*, 1997] show a discontinuous transform disrupted by three short segments (~10–20 km) called intratransform ridges (ITR), whose length decreases from west to east [*Rusby*, 1993]. Small ridge segments offset by a major transform fault have also been observed along certain parts of the East Pacific Rise such as the Siquieros, Quebrada, Gofar, Wilkes, and Garrett fracture zones [*Fox and Gallo*, 1984; *Lonsdale*, 1989]. However, in a slow spreading rate environment, such as Equatorial Atlantic, the St. Paul FZ case is unique. The nature of the St. Paul's ITRs is not clear. For example, do they represent pull-apart basins or en echelon relay zones? Concerning this question, *Schilling et al.* [1994, p. 1206] wrote

> The lack of well developed north-south magnetic anomalies at the equator and the tectonic complexity prevent us from deciding whether these relay zones represent the loci of seafloor spreading sustained over long periods of time or whether the volcanism is ephemeral and reflects leaky transform faults .. or oscillatory spreading...

During the St. Paul cruise, several dives by the submersible Nautile observed and sampled different structures of the St. Paul FZ [*Hékinian et al.*, 1998, 2000]. In the eastern ITR area (Figure 3), six dives (SP1-6), three deep-towed bottom camera profiles (SC1-3), and a detailed magnetic survey were carried out. This short (10–15 km in length) axial depression exhibits a general N-S orientation (340°). The axial depression deepens and broadens north and south into two sedimented nodal basins more than 5000 and 4800 m deep, respectively. Each basin is bounded by an E-W transform wall, and the axial valley is bounded on both sides by faulted rifted walls that reach up to 2800 m.

Figure 1. (opposite) (a) Satellite gravity map of St. Paul Fracture Zone [*Sandwell and Smith*, 1997] showing the studied area (box). The general location is displayed in the inset [*Smith and Sandwell*, 1994]. (b) Multibeam bathymetric map of the studied area (200 m contoured lines), obtained by R/V *N. Strakhov* in 1998 (courtesy of G. Udintsev and E. Bonatti). Near the top of the eastern wall, black star indicates the moored magnetic reference station. (c) Measured magnetic anomaly (colored area) before removal of a regional magnetic gradient, bathymetry (200-m contoured lines) and navigation tracks (medium lines, no data available along the dotted lines). Bold pink lines indicate the traces of the sections A, B, C used in Figures 2a–2c and 3d.

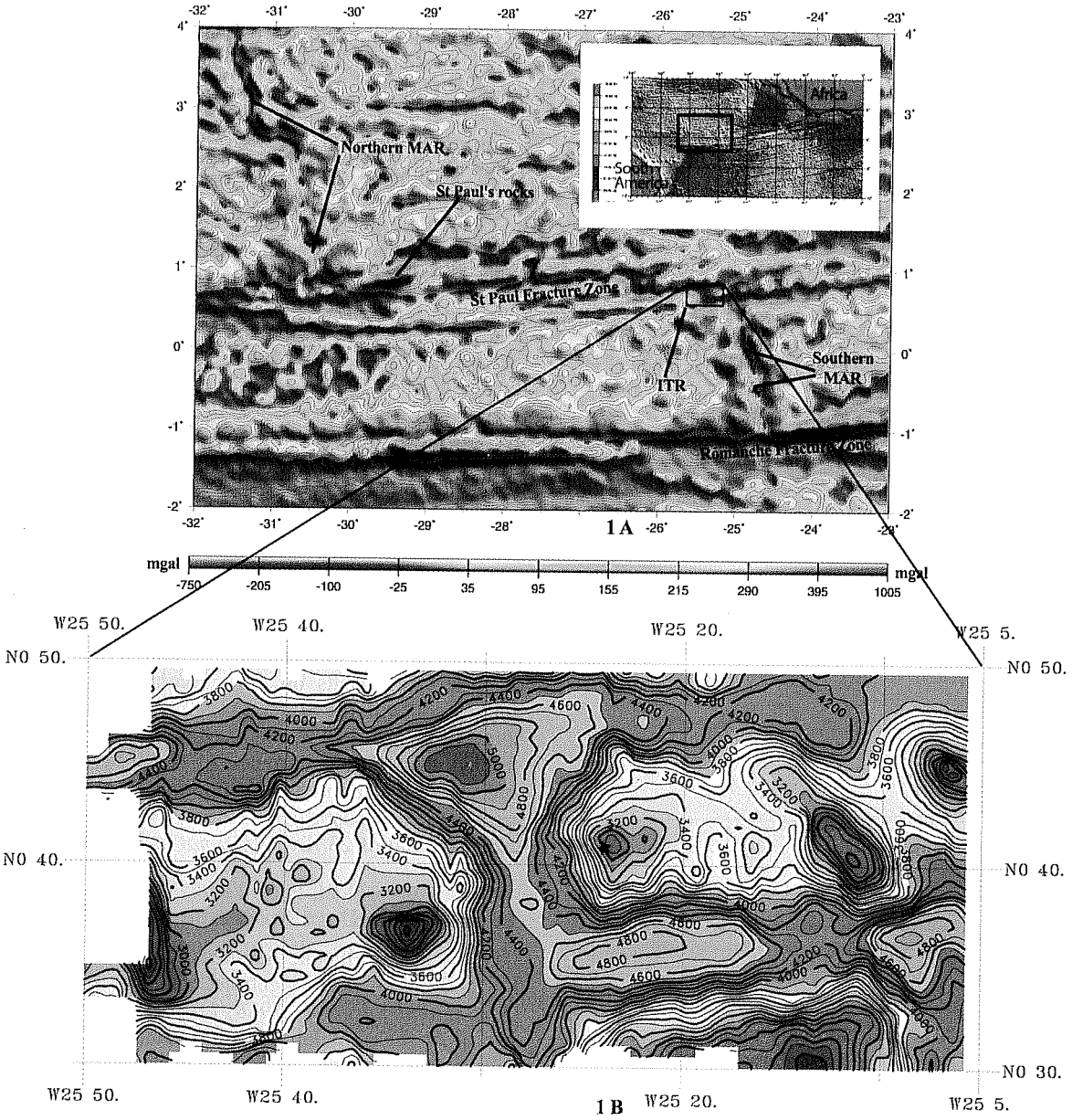
Northern MAR
St Paul's rocks
St Paul Fracture Zone
ITR
Southern MAR
Romanche Fracture Zone
Africa
South America
mgal
-750 -205 -100 -25 35 95 155 215 290 395 1005
W25 50.
W25 40.
W25 20.
W25 5.
N0 50.
N0 40.
N0 30.

1A

1B

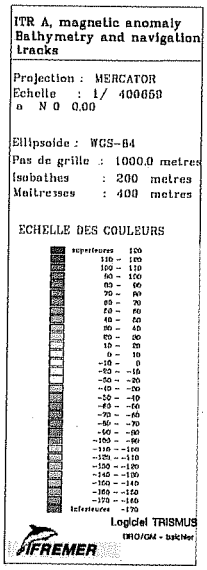
ITR A, magnetic anomaly
Bathymetry and navigation tracks
Projection : MERCATOR
Echelle : 1/ 400650
o N 0 0.00
Ellipsoide : WGS-84
Pas de grille : 1000.0 metres
Isobathes : 200 metres
Maitresses : 400 metres
ECHELLE DES COULEURS
Logiciel TRISMUS
IFREMER

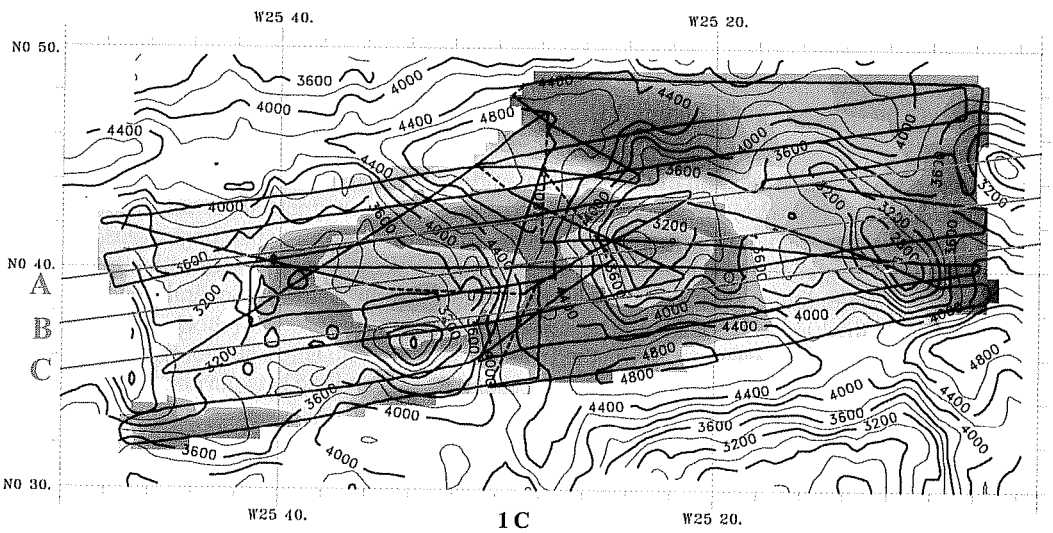
W25 40.
W25 20.
N0 50.
N0 40.
N0 30.
A
B
C

1C

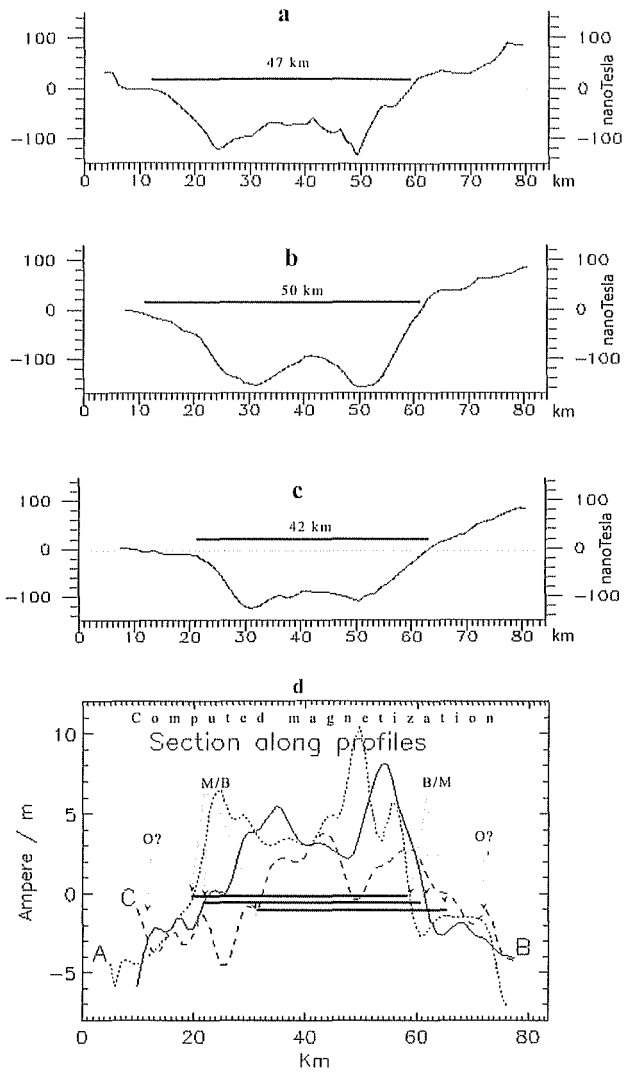

Figure 2. (a–c) Magnetic anomaly along the sections A, B, C (see Figure 1c). Thick lines show the positive central magnetic anomaly assumed corresponding to Brunhes anomaly (before removal of a regional magnetic gradient). (d) Equivalent magnetization along the sections A, B, C (see Figure 4d). Thick lines show the positive central magnetization area assumed corresponding to Brunhes area. The distances are projected on the X axis, so an easier comparison may be done with the Figure A1h.

[7] A composite geological section of the east flank of the axial valley, from 4500 m to 2840 m, was constructed from dives and bottom video-camera observations (Figure 3b). The rift valley floor displays fresh pillow lavas in the axial region exposed by N-S linear fissures, elsewhere, pelagic sediments (<15 cm thick) cover the floor. The neovolcanic zone is localized toward the eastern side of the rift valley, near the onset of the bounding wall faults. Between 4500 and 4200 m, several fresh talus piles, devoid of sediment, are located at the foot of steep faults. Between 4500 and 3900 m, at least five breaks in the slope were observed, marked by troughs around 20–30 m deep followed by gentle and sedimented slopes. These structures suggest recent normal faulting. The first outcrop of peridotites is found at 3970–4000 m, and they are associated with occasional basalts and diabase dikes. At shallower depth only, serpentinized peridotites and gabbros were observed and recovered in situ at various sites along the slope (Figure 3b). The transition between the peridotites and an upper volcanic section is marked by fresh basalt talus at ~2873 m depth. This volcanic section is located on a slope bounded by a small depression close to the top of the eastern wall at 2844 m depth and oriented in a 340° direction. The east-northeast facing slope and the sedimented floor of this depression consist of massive peridotite, while the opposite slope is made up of basalt debris. The west flank of the axial valley was not visited by submersible, but the deep-towed video-camera survey failed to show any volcanics. Moreover, during the last PRIMAR cruise on the *Academic Nicolaï Strakhov* in April 2000 [*Peyve et al.*, 2000; E. Bonatti et al., manuscript in preparation, 2002], dredge S2227 was carried out on the shallowest structure of the west flank (0°36.5′N, 25°34.0′W) and serpentinized peridotites and some fragments of massive talc of hydrothermal origin were recovered (D'Orazio et al., manuscript in preparation, 2002).

[8] In conclusion, the seafloor observations reveal an abundance of peridotites but only limited volcanics. The rift valley crust above 4000 m may be entirely built of peridotites and gabbros except for a thin cover of a few tens of meters of basalts on the summit of the east wall. In comparison with the St. Paul ITR, the MAR to the north and south of the 15°20 FZ, seems to be in a less magmatically starved state: The occurrence of basalts is more frequent, and ultramafic rubble mask important areas where gabbros are frequently suspected but were observed only twice during a total of 23 dives [*Cannat et al.*, 1997].

3. Magnetic Data Processing

[9] Near the equator, the intensity of the magnetic field is low and the equatorial electrojet enhances diurnal variations [*Roeser and Bargeloh*, 1988; *Forbes*, 1981; *Onwumechili*, 1967]. At such low latitudes, the identification of magnetic anomalies associated with long N-S structures is difficult because of the low anomaly amplitude. However, for short N-S structures, 3-D modeling may yield useful information about the magnetic sources if the low amplitude can be accurately mapped (see Appendix A). Therefore, in order to improve the accuracy of the magnetic survey, a Geometrics G856AX magnetometer was moored as a magnetic reference station at the center of the surveyed area, located on the east wall of the axial valley at ~2750 m, 200 m above the seafloor (Figure 1b). The reference station recorded the total magnetic field intensity each minute.

[10] Ten magnetic profiles, each ~35 nautical miles long, were made perpendicular to the axis of the valley (70°–250° heading). Several transverse profiles were also carried out in order to complete the survey and to check the discrepancies at the crossover points of two tracks [*Shu-Kun*, 1995] as an evaluation test for the quality of the survey. After corrections for the tow cable length and diurnal variations [*Riddihough*, 1971], the standard deviation of the 42 crossover point discrepancies is $\sigma_d = 6.1$ nT (before the removal of the diurnal variations the standard deviation was $\sigma_d = 9.1$ nT). Magnetic anomalies were then computed by removing the International Geomagnetic

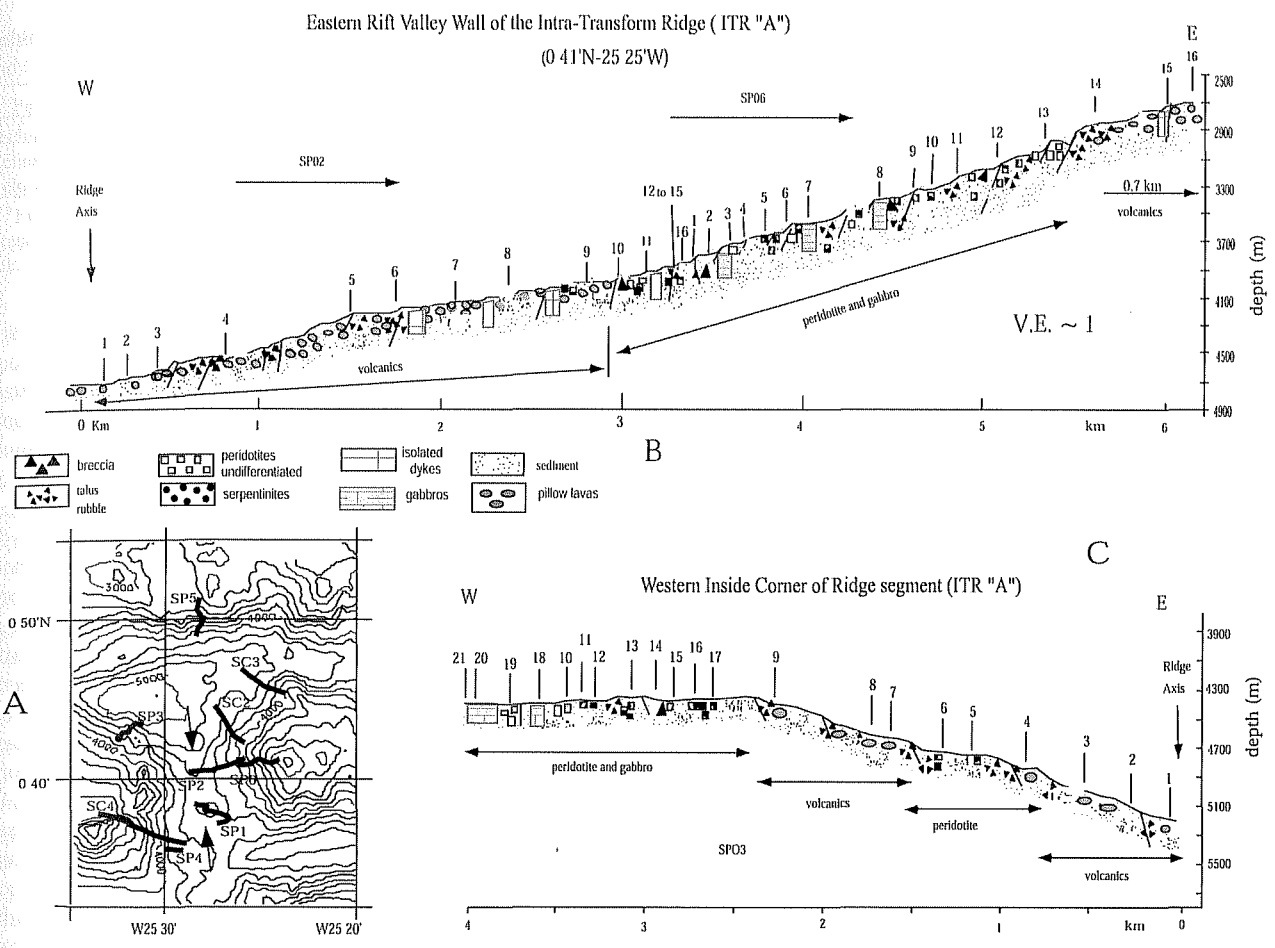

Figure 3. (a) Sketch map of the ITR showing the location of the submersible dives (SP1 to SP6) and the tracks of the deep towed video camera (SC2 to SC4). Black arrows indicate the rift valley. (b, c) Geological sections across the east wall of the rift valley and the western inside corner respectively, constructed from dives and deep towed camera observations [*Hékinian et al.*, 2000]. Note that the occurrence of sporadic and discontinuous volcanics which are mainly alternated with peridotites is confirmed on the west wall by the long SC4 section.

Reference Field (IGRF 1995, ftp.ngdc.noaa.gov). Then the magnetic anomalies were gridded to provide a digital terrain model on the same grid as the bathymetry (Figure 1c). In order to obtain a 1 km grid, a bilinear interpolation was performed. With such a fine grid, the effect of the bathymetry is better taken into account and the inversion instabilities, linked with the misfit between the true and the modeled bathymetry, are reduced. On the other hand, the number of unknowns increases and the resolution, perpendicular to the magnetic lines, obviously remains a function of their distance from the seafloor. All magnetic, gravity, or other parameter surveys carried out along discrete lines show some anisotropic data density. In the central part of the survey, several transverse lines reduce the anisotropy of data density and improve the resolution. A 2-D least squares adjusted planar trend has also been computed in order to remove any regional magnetic gradient and therefore balance positive and negative magnetic anomalies (Figure 4a).

[11] A generalized inversion method was applied to obtain the seafloor distribution of equivalent magnetization, [*Tarantola and Valette*, 1982; *Menke*, 1984; *Tarantola*, 1987]. This method is based on a linear discrete inversion taking as unknowns the magnetization of parallelepiped shaped prisms ($1 \times 1 \times 0.5$ km^3) which fit the bottom topography. Appendix A gives the general outline of the discrete inverse theory used here and the same approach, applied to gravity data, is described in some recent papers [*Camacho et al.*, 1997; *Bear et al.*, 1995; *Strykowski*, 1995]. Finally, we have to extract M from the general equation: $\mathbf{D} = \mathbf{G} \times \mathbf{M}$ (see Appendix A), where $\mathbf{D}$ is the data, $\mathbf{M}$ is the magnetization, and $\mathbf{G}$ is Talwani's coefficient matrix [*Talwani*, 1965]. The $\mathbf{G}$ coefficients are computed using two sets of parameters: (1) the relative geometry between each point of measure and the parallelepipedic cells and (2) the local features of the magnetic field (Tables 1a and 1b). In this case, the directions of the field and the magnetization are assumed to be the same. Finally, the symbol "$\times$" means the matrix multiplication.

[12] The $\mathbf{D} = \mathbf{G} \times \mathbf{M}$ equation represents an underdetermined system of 1711 data points (the gridded magnetic survey) and 3360 unknowns (the total grid of 40 rows

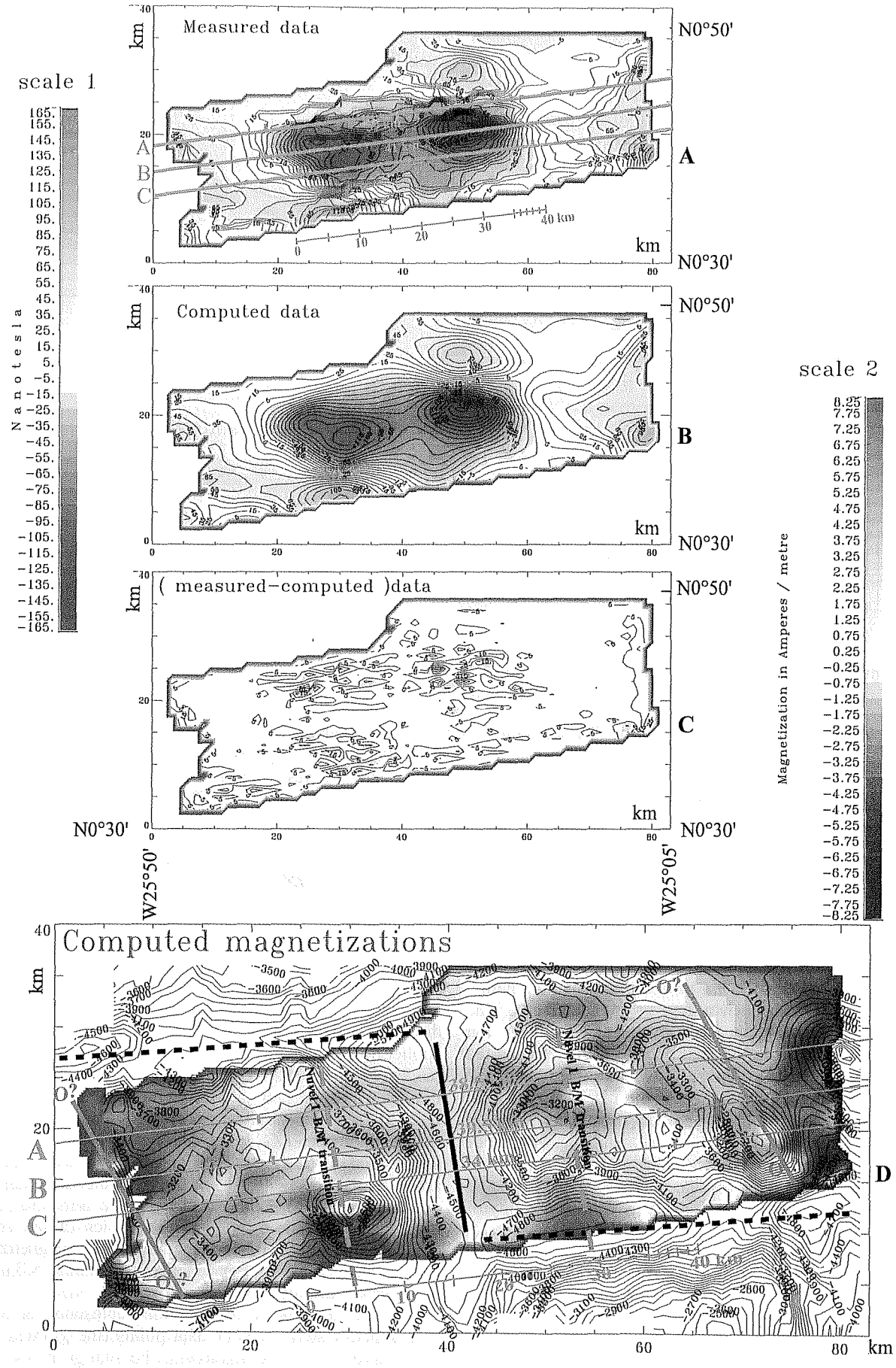
Measured data
Computed data
(measured−computed)data
Computed magnetizations
scale 1
Nanotesla
scale 2
Magnetization in Amperes / metre
N0°50'
N0°30'
W25°50'
W25°05'
km
A
B
C
D
40 km

Table 1a. IGRF 95 Parameters for 27 December 1997 at 00°40′N and 25°25′W[a]

Parameter	Value
Declination D	−18.05°
Inclination I	−16.21°
Field intensity F	28,275 nT

[a] Field intensity is not used in *Talwani*'s [1965] coefficients. The direction of the magnetization is assumed to be the same than that of the field.

Table 1b. Kinematic Parameters

Parameter	Value
Model[a]	NUVEL-1
Latitude pole	−39.4°
Longitude pole	62.5°
ω	0.32° Myr^{-1}
Latitude point	0.66°
Longitude point	−25.50°
Distance[b]	31.471 km Myr^{-1}

[a] *DeMets et al.* [1990].
[b] Full opening rate.

and 84 columns). In order to solve this problem, it is necessary to add some a priori information, such as a distribution law for the data d and the unknown values m (see Appendix A). Finally, we obtain the distribution of the magnetization through the display of the matrix **M** (Figure 4d). In order to check the results of the inversion, a recomputed field (called "computed data" on the Figure 4b) at each observation point is calculated from the equivalent magnetization intensities determined by the inversion and compared to the observed field (called "measured data" on Figure 4a). This residual difference is called the "deviation" (Figure 4c). At middle latitudes, inversions are generally performed with an assumed covariance model Cov **D** (see Appendix A) derived from the crossover point discrepancies. In the St. Paul area, if we use the same choice for Cov **D** (here $\sigma_d = 6.1$) as in previous studies [*Bideau et al.*, 1998], we obtain mathematical instabilities, such as the juxtaposition of cells with oscillatory magnetization values. It is assumed that such instabilities are a consequence of the low inclination of the magnetic field, which increases the mutual effect of a cell on its northern and southern neighbors. The first Gauss position produces a mutual effect twice as large as the second Gauss position as it is mainly the case at high latitude. Then, with Cov **D** acting as a damping parameter (see Appendix A), a higher value was looked for: after some trial and error, a value for Cov **D** corresponding to $\sigma_d = 6.1 \times 3 = 18.3$ was chosen. With this damping parameter the measured anomaly and the computed anomaly remain very close: The mean of the 1711 deviations is 0.34 nT, and the standard deviation is 7.14 nT, better than the input $\sigma_d = 18.3$ (Figures 4a, 4b, and 4c). Also, the equivalent magnetization distribution appears to be less oscillatory (Figures 4d). With the initial damping parameter $\sigma_d = 6.1$, the previous parameters are better (mean of 0.05 nT and the standard deviation of 5.45 nT), but in that case the magnetization distribution is more oscillatory: We have to choose a trade-off between resolution and continuity (see Appendix A). With the same horizontal gridding, different cell thicknesses were also tried. One configuration considers a 1-km-thick layer, and a second model has two layers, each 0.5 km thick. The nonuniqueness of the potential field methods means that horizontal magnetic or gravimetric surveys are not able to discriminate between various vertical distributions of magnetic or density sources. The different vertical configurations provide quite similar solutions in terms of horizontal contrasts and only the intensity of magnetization differs. It was observed that inversion instabilities decrease when the thickness decreases. For this reason and also for the a priori choice of σ_m, the solution with a thickness of 0.5 km was chosen.

[13] Among the 1711 measured points only 2 show a deviation $\gtrless \pm 2\ \sigma_d$ (36.6 nT) and 40 show a deviation $\gtrless \pm \sigma_d$ (18.3 nT). The deviations of more than 90% of the area are in the interval ±15 nT (Figure 4c, color scale 1). The extreme magnetizations values are $m = -12.5$ A m^{-1} and $m = +12.9$ A m^{-1}, which is consistent with the assumed standard deviation $\sigma_m = \pm 10$ A m^{-1}. All these features are obviously in agreement with the initial Gaussian distribution assumptions. The larger residual errors are often distributed on the steep slopes where the fit of parallelepiped cells to the topography is rather poor.

[14] If the average magnetization is $m_0 = 0$ (a priori data, see Appendix A), the average of the absolute values of equivalent magnetization is $\langle |m| \rangle = 2.7$ A m^{-1}. When normalized by the magnetic field (Table 1), this value becomes

$$\aleph_{\text{St-Paul}} = \langle |m| \rangle / F = 2.7/28275 = 9.6 \times 10^{-5} \text{A m}^{-1}\text{nT}^{-1}.$$

We observe that $\aleph$ obtained on a little less starved ridge segment of the MAR, located at 34°N [*Bideau et al.*, 1998], performed under a similar cell gridding and with the corresponding value of F, is quite close $\aleph_{34°N} = 10.3 \times 10^{-5}$ A m^{-1} nT^{-1}. We think that such a parameter, dimensioned as an effective magnetic susceptibility, could represent the

Figure 4. (opposite) Colored area corresponding to magnetic parameters. Color scale 1 is relative to Figures 4a, 4b, and 4c. Color scale 2 is relative to Figure 4d. Coordinates $x = 0$, $y = 0$ correspond to 0°30′N and 25°50′W. Axes calibrated in km. (a) Measured magnetic anomaly after removal of IGRF and a regional planar trend. The width of the negative anomaly assumed corresponding to Brunhes area is indicated along the three sections A, B, C. (b) Computed data of the expected magnetic anomaly calculated from bathymetry and magnetizations obtained by inversion (Figure 4d). (c) Distribution of deviations equals measured minus computed data. (d) The bathymetric map (100-m contoured line) is superimposed on the distribution of calculated magnetizations as a result of the inversion with a priori data (see text). Magnetization along sections A, B, C is displayed in Figure 2d. Bold black line indicates the valley axis, and dotted bold black lines show the assumed trace of fracture zone. Solid green lines mark the possible anomaly 2 (Olduvai event) and dotted green lines indicate the theoretical limits of Brunhes area according to the NUVEL-1 model. Note the extension of the positively magnetized area which is largely beyond the dotted green lines.

capacity of the seafloor to contribute to the sea surface anomalies.

4. Discussion

[15] The NUVEL-1 model for the African and South American plates (Table 1) [*DeMets et al.*, 1990] indicates a total spreading rate of 31.47 mm yr^{-1} for the studied area, i.e., a total opening of 24.5 km during the Brunhes chron (780 ka). After the inversion of the data described above, the width of the positive central magnetized area, measured perpendicularly to the axial valley of the ITR is estimated to be ~37 km (38.5, 39.5, and 34 km on the sections A, B, C, respectively, Figures 2d and 4d). The accuracy of determination is estimated at 2 × 1 km corresponding to the size of the elementary cells at each extremity. Assuming that this central anomaly corresponds to the normal Brunhes epoch, the total opening is at least 37-2 = 35 km and the opening rate is 35×10^6 mm/0.78×10^6 years = 44.87 mm yr^{-1}. This opening rate is more than 40% too high with respect to the NUVEL-1 model. This means that, at least locally, an anomaly in the recording mechanism of the Earth magnetic field by the seafloor is likely to exist. Moreover, in previous studies [*Bideau et al.*, 1998; *Sichler et al.*, 2001] near 33°50′N and 35°N on the MAR, we found, with the same approach, that the width of the positively magnetized central area fitted fairly well with the Brunhes anomaly given by the NUVEL-1 model. Inversely, for the studied St. Paul's ITR, a large difference between the observed and predicted spreading rates is noted. Such a difference is assumed to be significant and needs explanation.

[16] Three kinds of hypothesis are formulated: (1) An episode of fast spreading occurred in this area during the Brunhes epoch. (2) The magnetic record is not continuous and could be a consequence of the "oscillatory spreading" or "repeated ridge jumping." (3) The lateral limits of the positive magnetized body are not isochrons (in fact, the contour of the positively magnetized central area is quite apart from a simple path more or less parallel to the central valley as an isochron should to be: southward the area become more and more asymmetrical in regard of the axial valley and everywhere the contour displays a rather random course not directly in relation with an isochron, Figure 4d).

1. If an episode of fast spreading occurred in this area during the Brunhes epoch, the distance between the two following anomalies would also have recorded this episode. But the distance between the two (unfortunately not well defined) chron 2 anomalies (Olduvai event = 1.86 Ma) [*Cande and Kent*, 1995] is ~61 km (Figure 4d), indicating a 32.8 mm yr^{-1} spreading rate, which is fairly close to the rate given by the kinematic model (31.47 mm yr^{-1}). So, in order to match this difference, a rapid succession of slow and fast spreading episodes during the last 1.86 Myr has to be envisaged. If the ambiguous anomaly 2 argument is not retained, a comparable process of slow and fast phases is to be assumed in order to accommodate the mean opening rate. Such a process of "elastic rebound" was invoked for the rapid extension of the Asal rift (Afar) during the Ardoukoba volcano tectonic event in 1978 [*Tarantola et al.*, 1979; *Ruegg et al.*, 1984] and for the opening of the Atlantis II Deep in the Red Sea [*Le Quentrec and Sichler*, 1991]. However, the first example concerns a continental rift and the second one is related to the initial phases of oceanic opening where the steady state is not reached. Here, in a pure oceanic, "steady state" context, such a mechanism is rather unlikely. In the specific context of a short axial segment "jammed" between two long transforms, however, anomalous behavior cannot be totally excluded (see hypothesis 2).

2. Curious features have been reported in the Atlantic equatorial region for 30 years, particularly by Italian and Russian authors [*Bonatti and Honnorez*, 1971; *Bonatti and Crane*, 1982; *Bonatti et al.*, 1996; *Kepezhinskas*, 1990; *Rohr*, 1996; *Udintsev et al.*, 1990]. They are related with relics of continental mantle or old continental rocks on the islets of St. Paul and in the Doldrums FZ, or with lower Cretaceous limestone in the Romanche FZ. All these rocks were found on much younger seafloor. In order to explain these anomalies the concept of oscillatory spreading or repeated ridge jump was proposed by E. Bonatti and others [*Bonatti and Honnorez*, 1971; *Bonatti and Crane*, 1982; *Bonatti et al.*, 1996; *Rohr*, 1996]. Within this framework, our observations may thus be simply explained. The width of the positively magnetized central body could correspond to the record of a longer normal chron than Brunhes or more likely to two successive normal chron (for example, Brunhes and Jaramillo) but without the negative record between them. At this time, a ridge jump would had occurred and then the corresponding negative area would be expected to an other ITR. In a continuous accretion process of the seafloor, the forward modeling does not support any merging of Brunhes and Jaramillo which broadens the width of Brunhes at the level 0 A m^{-1} (see Figures A1g and A1h).

3. Dive observations show that exposures of serpentinized peridotites and gabbros largely predominate on the axial valley flanks of the ITR, so they are the main candidates for the origin of the magnetic anomalies. In hole 735B, gabbros must contribute to the magnetic anomalies with average stable remanent magnetization up to 1–2 A m^{-1} [*Pariso and Johnson*, 1993]. Altered gabbros have been observed as carriers of very stable remanence [*Dunlop and Prevot*, 1982]. Highly magnetized serpentinized peridotites, up to 11.5 A m^{-1} [*Fox and Opdyke*, 1973] or 20 A m^{-1} [*Dunlop and Prevot*, 1982] previously reported from different regions of the Atlantic Ocean, can potentially represent a source of magnetic anomalies. In hole 504B, between 1 and 2 km depth, two kinds of delayed secondary magnetization appear to have been acquired by the sheeted dike complex at 300–400°C in ~2.5 Myr with a strong probability of recording several polarities [*Hall and Muzzatti*, 1999]. Opinions remain divided about the contribution of these deep layers on lineated magnetic anomalies. Some authors think that serpentinization is a complex and irregular process and even if the measured samples carry NRM comparable to the NRM of altered basalts, they are not reliable candidates for preserving the magnetic signal [*Nazarova*, 1994; *Lienert and Wasilewski*, 1979]. Other authors [*Tivey and Tucholke*, 1998], studying the differential decay of the anomalies between the center, the ends and the corners of a segment, have shown that, off axis, the contribution of serpentinized rocks is unavoidable. At 20–24°N, on the MAR, during some amagmatic phases of spreading, high magnetization values were associated with detachment faults outcropping gabbros and peridotites

which experienced serpentinization, but the question of overprinted and delayed magnetization was not tackled [*Pockalny et al.*, 1995]. From another perspective, satellite magnetic studies also show that the extrusive layer alone is not capable of generating the entire magnetic signal and that the contribution of deeper crustal sources is necessary [*Dyment and Arkani-Hamed*, 1998; *Purucker and Dyment*, 2000].

[17] During serpentinization, magnetite grains are produced. The high susceptibility of serpentinized peridotites producing an induced magnetization of the same magnitude as the remanent magnetization [*Fox and Opdyke*, 1973; *Pariso et al.*, 1996] could also provide some partial explanation for the magnetic observations in the St. Paul area. We suggest another process: as the serpentinization of some equatorial Atlantic peridotites involves low temperature hydration from 200°C to 30°C to form magnetite [*Bonatti et al.*, 1984] a thermochemical or a chemical remanent magnetization may be acquired with the help of processes associated to the spreading. This could take place by detachment faults, close to the accretion axis [*Lagabrielle et al.*, 1998; *Tucholke and Lin*, 1994; *Tucholke et al.*, 1998] and by vertical tectonics at some distance from the axis.

[18] The thermal state of the first hundred meters of the oceanic floor generated at slow spreading ridges is unknown and not yet modeled. Consequently, we assume that serpentinization depends essentially on water penetration, which is triggered by tectonic strains. If the observed magnetization arose from an acquisition process during the serpentinization, then the magnetization would not only be coupled with the emplacement of the seafloor, as it is for the extrusives, but would depend on its hydration history during and after its emplacement. Close to the axis, incipient serpentization occurs at the depth of the fragile-ductile boundary. This serpentinization, favored by water penetration during each tectonic event, will progress upward and laterally until the tectonic activity vanishes and the cracks seal. So, at each phase of serpentinization, a new magnetization is added to the previous one. If a reversal of the magnetic field occurs, the new polarity would overprint a new magnetization on an older one. Then, at a distance from the center of the rift valley, where tectonic deformation vanishes, seawater penetration is reduced and serpentinization will progressively stop and the initial magnetization will be preserved. Active tectonic deformation may occur at a distance of 15–20 km from the axis, as it was shown in the south of Atlantis FZ at 29°N [*Escartín et al.*, 1999]. This distance is compatible to the half of the width of the positively magnetized area, observed here (~35/2 = 17.5 km, Figure 4d, as mentioned above). As an illustration, we observe the normally magnetized structure (the area of dredge site during PRIMAR cruise) lying on reversely magnetized seafloor near the western limit of the direct-inverse magnetized zone (X = 30 km, Y = 12.5 km, Figure 4d). The positively magnetized top of the structure could result of the serpentinization of an initially negatively magnetized area, favored by tectonic uplift. The negatively magnetized surroundings would represent the relics of previous magnetization.

[19] A variation of this scenario could be based on the amount of the induced magnetization in the serpentinites instead of the chemical remanent magnetization. The abnormal extension of the positively magnetized area could be the result of an overprint of a strong induced magnetization on previously already reversed magnetized rocks. Such a masking effect has been proposed at 29°N in the Atlantic, for the magnetic anomalies marking the second order discontinuity traces, which disappear after the Matuyama-Gauss boundary [*Pariso et al.*, 1996]. In the St. Paul area the masking effect would be strong enough to reduce the size of the weakly negative magnetized area, but the more negatively magnetized area would nevertheless keep its polarity.

[20] As a result of this, serpentinites contribution hypothesis to magnetization, we infer that a blurring effect on the magnetic anomalies limits may be expected in the serpentinites rich seafloor area. So, for the studied ITR, the merging of Brunhes and Jaramillo, if it occurs, is itself unexpected with respect of the classical theory of seafloor spreading (compare Appendix A "method efficiency" and Figures A1f and A1h). This kind of recording anomaly is the subject that we have emphasized.

5. Conclusion

[21] The present study shows that magnetic anomalies can be detected along short accreting ridge segments of the Equatorial region. The ITR represents a short spreading ridge segment. The features of a centered Vine-and-Matthews-like magnetic anomaly suggest a relay zone. Moreover, the presence of two deep basins in the north and south of the studied segment recalls nodal basin morphology, which does not agree with the 3-D modeling of a pull-apart example [*Katzman et al.*, 1995].

[22] In a more magmatically active ridge, such as the MAR at 25°30′–27°10′N, the crustal magnetization is mainly due to the axially extruded lavas. However, off-axis, the magnetization of the lower crust and/or upper mantle transition, possibly due to serpentinization, could become the important source of the magnetic anomalies [*Tivey and Tucholke*, 1998]. In this study, we show that a Vine-Matthews-type magnetic anomaly is present in a starved ridge context. We suggest that this central magnetic anomaly probably has its origins in the serpentinized peridotites through a chemical or thermochemical process that is not synchronized with their emplacement, but rather depends on the extent of water penetration linked to tectonic activity along boundary normal faults. While delayed magnetization was previously described in vertical sections of ODP cores [*Hall and Muzzatti*, 1999], the excess of the positively magnetized area on the eastern ITR of the St. Paul would be the first observation of a delayed magnetization made on a horizontal scale. If this assumption is retained, this phenomenon could act elsewhere, as a blurring parameter for the Vine-Matthews anomalies where serpentinized peridotites are present in a thin crust context. If the hypothesis of a strong induced magnetization was at the origin of our observations, the consequences will not be preserved over a change of magnetic polarity. The hypothesis of the oscillatory spreading is attractive, but yet remains highly speculative. Nevertheless, this could be tested in the future with a simple check on the two other short ITRs. The same magnetic patterns than that of the studied ITR will support the concept of delayed magnetization in a magmatically starved context, inversely, different but always anomalous

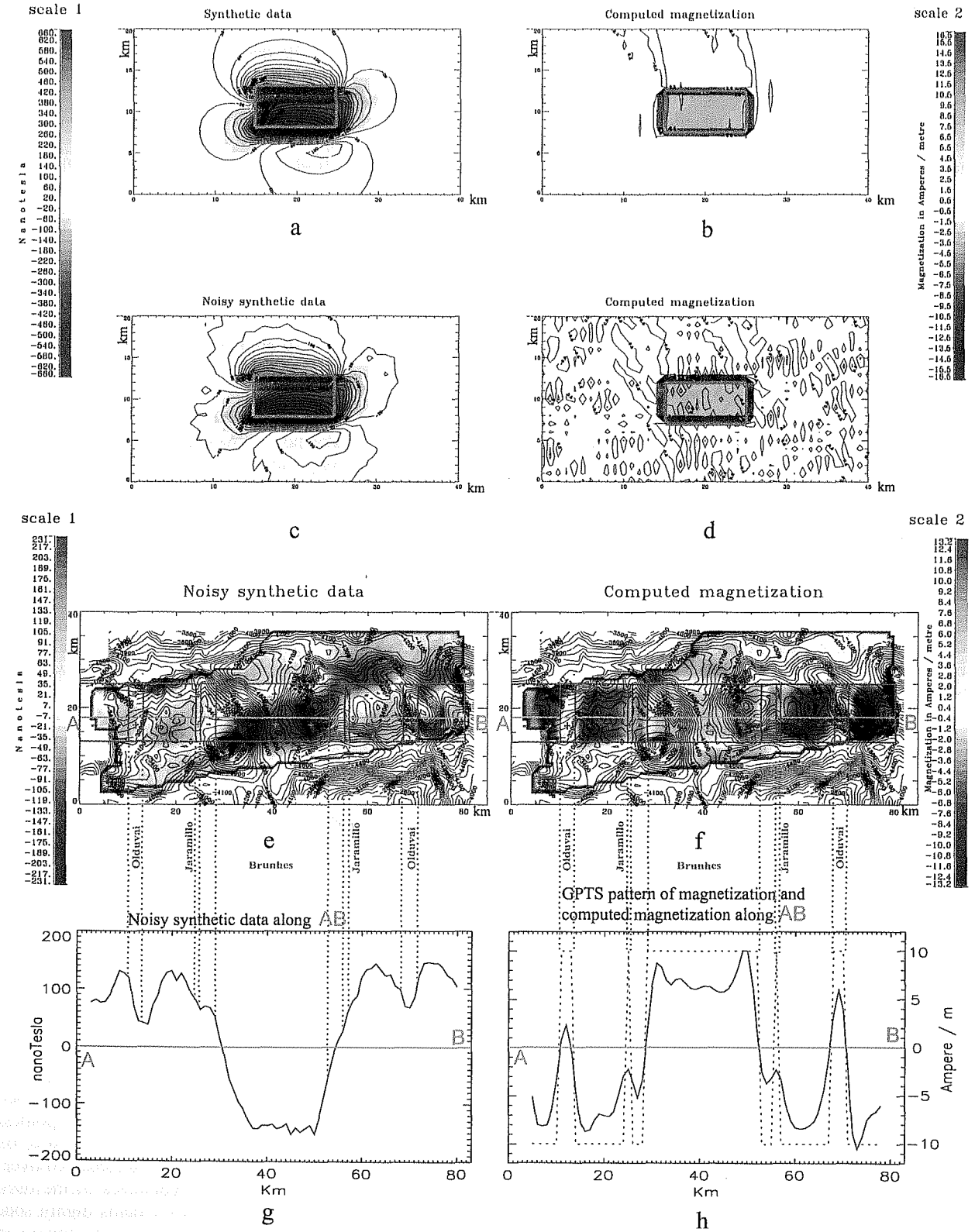
scale 1
Synthetic data
Computed magnetization
scale 2
Nanotesla
Magnetization in Amperes / metre
km
a
b
Noisy synthetic data
Computed magnetization
c
d
scale 1
scale 2
Noisy synthetic data
Computed magnetization
Olduvai
Jaramillo
Brunhes
e
f
Noisy synthetic data along AB
GPTS pattern of magnetization and computed magnetization along AB
nanoTesla
Ampere / m
Km
g
h

magnetic patterns could be a clue for *Bonatti and Crane*'s [1982] hypothesis if they were mutually complementary.

Appendix A

A1. Main Outline of the Generalized Inverse Method

[23] The seafloor in the surveyed area was divided into elementary parallelepiped shaped cells, which follow the bottom topography. The edges of the juxtaposed elementary cells are oriented northward, eastward and downward. Let m_j be the magnetization of the jth cell and d_{ij} be the magnetic effect of cell j at the point i where a magnetic measurement was made. We obtain the linear relation $d_{ij} = g_{ij*}m_j$, where g_{ij} is a coefficient calculated according to *Talwani*'s [1965] algorithm. All the j cells provide at the i point a magnetic anomaly $D_i = \Sigma_j d_{ij} = \Sigma_j g_{ij*}m_j$.

[24] In matrix notation the previous linear relation becomes

$$\mathbf{D} = \mathbf{G} \times \mathbf{M},$$

where $\mathbf{D}$ is the k row and one column data matrix, or the data vector (magnetic anomaly), $\mathbf{M}$ is the l row and one column magnetization matrix or the magnetization vector, and $\mathbf{G}$ is the k row and l column, the "data kernel" [*Menke*, 1984], also-called the Talwani coefficient matrix and "$\times$" means the matrix multiplication.

[25] G is calculated for all the j cells and the i points, using the magnetic field parameters, given by the IGRF model (Table 1a). In order to obtain the matrix $\mathbf{M}$, knowing $\mathbf{D}$ and $\mathbf{G}$, when the problem of inversion is underdetermined (i.e., if $k < l$), it is necessary to add some a priori information, such as a distribution law for the data d and the unknown values m. If a simple Gaussian law is assumed for the data and the unknown values, the matrix $\mathbf{M}$ is given by the following formula [*Menke*, 1984]:

$$\mathbf{M} = \mathbf{M_0} + \mathbf{G}^{-g} \times \{\mathbf{D} - \mathbf{G} \times \mathbf{M_0}\}, \quad \text{(A1)}$$

where

$$\mathbf{G}^{-g} = \text{Cov } \mathbf{M} \times \mathbf{G}^{T} \times \{\text{Cov } \mathbf{D} + \mathbf{G} \times \text{Cov } \mathbf{M} \times \mathbf{G}^{T}\}^{-1}. \quad \text{(A2)}$$

$\mathbf{G}^{T}$ is the transpose of $\mathbf{G}$, Cov $\mathbf{M}$ is the covariance of the magnetizations distribution, and Cov $\mathbf{D}$ is the covariance of the data distribution. $\mathbf{M_0}$ is the a priori matrix of magnetizations distribution, known by its mean value and its standard deviation. Equation (A2) is called the "generalized inverse."

[26] Here the following are assumed:

1. $\mathbf{M_0} = m_0 \times \mathbf{I}$, where $\mathbf{I}$ is the identity matrix and $m_0 = 0$ is the mean magnetization since the anomalies are balanced. Since each magnetization m_j and each data D_i is independent from each other, the a priori models of magnetization and data are uncorrelated, and their covariances are reduced to variances such as

$$\text{Cov } \mathbf{M} = \sigma_m^2 \times \mathbf{I},$$

$$\text{Cov } \mathbf{D} = \sigma_d^2 \times \mathbf{I}.$$

2. The standard deviation $\sigma_m = \pm 10$ A m^{-1} is a classical interval of magnetization values, often found for mid-oceanic ridge floor [*Hall and Muzzatti*, 1999; *Sempéré et al.*, 1990].

3. The standard deviation of the crossover point discrepancies is $\sigma_d = 6.1$ nT.

[27] Since all the members of equations (A1) and (A2) are known, $\mathbf{M}$ can be computed.

[28] Note that equation (A1) may be reduced to $\mathbf{M} = \mathbf{G}^{-g} \times \mathbf{D}$ since the data and the unknowns follow centered Gaussian law (mean of 0). An a priori offset of the distribution $\mathbf{M}$ requires the explicit formula of equation (A1). An offset of the $\mathbf{D}$ distribution (zero line of the magnetic anomalies) acts as a kind of complex annihilator and introduces bias in the $\mathbf{M}$ distribution. Before the regional gradient removal, the magnetic anomaly data mean is -13 nT, its SD (standard deviation) is 62 nT, the

Figure A1. (opposite) Synthetic data relative to Appendix A. The axes are in km. The pink boxes indicate the location of the magnetized body. Declination and inclination are given in Table 1a. (a) Magnetic field created by a positively magnetized body of 4km wide, 10 km long and 1 km thick with a magnetization of 10 A m^{-1}, at 1 km above the upper side of the body. Scale color 1, upper. (b) Distribution of computed magnetization as the result of inversion of the "synthetic data" (see text for the a priori of the inversion method). Scale color 2, upper. (c) Magnetic field created by a magnetized body, same as Figure A1a, added with a Gaussian noise (see text for the features of the noise). Scale color 1, upper. (d) Distribution of computed magnetization as the result of inversion of the "noisy synthetic data".(see text for the a priori of the inversion). Scale color 2, upper. (e) Magnetic field created by alternatively normal and inverse magnetized bodies according to the geomagnetic polarity timescale and the theoretical rate of opening. The north-south extension of the magnetized bodies is 12 km, thickness is 0.5 km, magnetization is alternatively +10 and -10 A m^{-1}. The synthetic magnetic field is added with a Gaussian noise (see text for the features of the noise). The magnetized bodies fit the topography of the St. Paul FZ study area. The size of each parallelepiped cell is of $1 \times 1 \times 0.5$ km^3. Scale color 1, lower. (f) Distribution of computed magnetization as the result of inversion of the noisy synthetic data (see text for the a priori of the inversion method). Scale color 2, lower. (g) The profile along the green line AB in Figure A1e shows that the width of the negative anomaly is 24 km and corresponds exactly to the width of the Brunhes area given by the kinematic model. The negative anomaly is slightly shifted eastward. (h) Profile along the green line AB in Figure A1f shows the theoretical distribution of magnetization (dotted line) and the distribution of magnetization as the result of the inversion of the synthetic noisy data (solid line). The both curves indicate 24 km for the width of the Brunhes area. The Jaramillo events are too narrow to produce positive anomalies at the sea level. In these conditions, the 3-D model does not support any coalescent effect between Brunhes and Jaramillo. Olduvai events produce well-defined positive anomalies.

magnetization mean is +0.8 A m^{-1} and its SD is 3.6 A m^{-1}. After this correction the data mean is obviously almost 0 (1.8×10^{-5}), its SD is smaller (53 nT), the magnetization mean is −0.3 A m^{-1}, and its SD is 3.3 A m^{-1}. These values illustrate that in this case, a shift, which makes the magnetic anomaly data slightly more positive, produces more negative equivalent magnetizations. Since the "absolute" zero line of the data is unknown (the potential is defined except for a constant), some uncertainty remains with the magnetization. Nevertheless, the magnetization contrasts are preserved in any case (see below the forward synthetic models) and the balancing of anomalies produces magnetization limits which fit fairly well the magnetization contrasts. Moreover, it is easier to compare real magnetic data statistically balanced with the forward synthetic models which do not display any offset of the zero line. It is for these two independent reasons that a regional gradient is systematically removed.

A2. Meaning of Cov D and Cov M

[29] In probability theory, Cov **D** measures the correlation between **D** joint distributions. Here each datum is assumed to be a distribution **D** characterized by its mean value d and its standard deviation σ_d. The covariance of a datum with itself is the variance σ_d^2. Then if the data are uncorrelated, the matrix covariance is reduced to the first diagonal, and if the data are defined with the same variance, Cov $\mathbf{D} = \sigma_d^2 \times \mathbf{I}$.

[30] In our inversion problem, Cov **D** may be intuitively seen as a parameter which determines the goodness of fit: if Cov **D** increases, the goodness of fit decreases and a smoother solution is found. More strictly, Cov **D** acts as a damping parameter, since it enhances the main diagonal values of the square matrix $\{\text{Cov } \mathbf{D} + \mathbf{G} \times \text{Cov } \mathbf{M} \times \mathbf{G}^T\}$ in equation (A2). Therefore the main diagonal of $\{\text{Cov } \mathbf{D} + \mathbf{G} \times \text{Cov } \mathbf{M} \times \mathbf{G}^T\}^{-1}$ is also enhanced, and the final solution is more stabilized.

[31] The same general argument holds true for Cov **M**, but its place in equation (A2) is different. Cov **M** acts as a scale factor and gives the width of the Gaussian distribution of magnetization in which the solution is to be found.

A3. Method Efficiency

[32] Some forward synthetic models were carried out and then inverted in order to check the limits of this approach. In all the cases, we used the same parameters ($I = -16.2°$ and $D = -8.05°$ and Cov **D** and Cov **M**) as those for the studied area. First, a very simple geometric model was used: a parallelepiped-shaped block of 4 × 10 × 1 km^3 northward, eastward, and downward, respectively, at a depth of 1 km with a magnetization $M = 10$ A m^{-1}. This block generates a magnetic "synthetic anomaly" and the result of the inversion of this anomaly is displayed (Figures A1a and A1b, respectively). Afterward, at the next step, a Gaussian noise of mean 0 and $\sigma_d = 6.1$ nT is added to the previous anomaly (Figure A1c). A new inversion is then performed and the results are displayed in Figure A1d. The last step is a more realistic simulation. With the true bathymetry of the studied area, magnetized blocks of alternatively −10 and +10 A m^{-1} were juxtaposed according to the geomagnetic polarity timescale (GPTS) [*Cande and Kent*, 1995], and the NUVEL-1 opening rate [*DeMets et al.*, 1990]. The magnetized blocks are centered on the axial valley ($X = 40$ km) and extend northward from $Y =$ 13 to 25 km. With the used size of elementary cells in the computation (1 × 1 × 0.5 km^3), the width of the magnetized bodies are corrected to the nearest whole number, so the width of the Brunhes area is 24 km, Jaramillo area is 1 km, and Olduvai area is 3 km. The chron C2r.1n [*Cande and Kent*, 1995], between 2140 and 2150 ka (0.150 km width), is ignored (Figure A1h, dotted line). A Gaussian noise with the same features was added to the computed synthetic anomaly (Figure A1e) and the inversion performed (Figure A1f). Figure A1g displays a cut in Figure A1e along line AB. The initial model of magnetization and the result of inversion along AB are shown as dotted and solid lines, respectively, in the Figure A1h. It is easy to see (Figure A1h) that the width of the Brunhes area obtained by inversion (solid line) is exactly the same as that of the initial model at the level 0 A m^{-1}. The Jaramillo events do not appear as positive magnetization but only as less negative areas with no effect on the width of the Brunhes at the level 0 A m^{-1} (Figure A1h). Then the forward model used here does not support any widening effect of Brunhes by Jaramillo. These three inversions used the same starting values: $m_0 = 0$ and $\sigma_m = \pm 10$ A m^{-1}. The distribution of magnetization in these synthetic examples is far from a Gaussian distribution assumed by the method. For the two first examples the extreme values of magnetization deduced from inversions are 10.4 and −0.9 A m^{-1} (Figure A1b) and 11.7 and −2.3 A m^{-1} (Figure A1d) instead of 10 and 0 A m^{-1} on and off, respectively, the magnetized blocks. For the third example the extreme magnetizations are −11.8 and 10.8 A m^{-1} on the magnetized blocks and −5.6 and 4.5 A m^{-1} off the magnetized blocks (instead of −10, +10, and 0 A m^{-1}). The effect of $\mathbf{M_0}$ as a starting value is to reduce the discrepancies between the expected values and the "true" values as m_0 distribution comes close to the departure value distribution (equation (A1)). Nevertheless, the limits of the magnetic contrasts are always well respected. These considerations enable the introduction of the annihilator concept: theoretically, the problem of nonuniqueness is solved by the minimization of the vector length representing the solution with the a priori data and unknowns distribution features. So the annihilator is not as useful as in the methods based on the Fourier transforms [*Parker and Huestis*, 1974]. Nevertheless, equation (A1) may be written

$$\mathbf{M} = \mathbf{G}^{-g} \times \mathbf{D} + \{\mathbf{I} - \mathbf{R}\} \times \mathbf{M_0}, \qquad \text{(A3)}$$

with $\mathbf{R} = \mathbf{G}^{-g} \times \mathbf{G}$ and **I** the identity matrix.

[33] **R** (called the model resolution matrix) never equals the identity matrix in an underdetermined problem [*Menke*, 1984], so in order to obtain something like the annihilator, equation (A3) may be used in a reduced form since $\mathbf{D} = 0$ (annihilator definition). For each a priori distribution $\mathbf{M_0}$, the "pseudo-annihilator" is $\mathbf{M} = \{\mathbf{I} - \mathbf{R}\} \times \mathbf{M_0}$. Here, in practical application of the theory, the annihilator is not useful since the means of the a priori models of data and magnetization are zero.

[34] In the synthetic cases shown here, there is a real discrepancy between "real data" distribution and the theory

assumptions; nevertheless, the results show the robustness of the generalized inverse method.

A4. Edge Effects

[35] The inversion system used here introduces insignificant edge effects since the bathymetric survey largely overlaps the magnetic survey: each cell of the grid participates in the calculation of the model anomaly even if no magnetic anomaly value is attached to it. In other words, this is the reason why the problem is underdetermined: There are more unknowns than equations, and **G** is not a square matrix. So, the "edge effects" are rejected outside the area of the magnetic survey and are localized on the edges of the bathymetric survey. An edge effect ought to be present only where the edge of the bathymetric survey is close to the edge of the magnetic survey such as in the north of the surveyed area from km 40 to km 80 (Figure 4c). Nevertheless, such an effect is not clearly visible in this region: where a bathymetric datum is missing on a node of the grid, a nonsignificant value is affected (as a flag), just a bit larger than the maximum bathymetric value. In this region, the nonsignificant values are fairly close to the true bathymetry, and therefore the edge effect is low.

[36] **Acknowledgments.** We are grateful to the captain, officers, and crew of the R/V *Le Nadir* for their help and patience during the St. Paul cruise. The careful handling of the magnetic sensors by the crew is particularly acknowledged. The help of R. Legall and A. Gourmelon of GENAVIR for the reconditioning, handling, and use of the deep-towed camera is also greatly appreciated. We are also grateful to the submersible Nautile's team for their expertise and encouragement during the diving operations. We thank D. Bideau for many discussions relating to petrology. We also thank M. Tivey, J. Gee, and J. Escartín for their constructive comments which contributed to the clarification and improvement of the manuscript during the review process. We are very grateful to F. H. Vine for his kind encouragement. We are thankful to W. Minor Davis (wmd@luna.ngdc.noaa.gov), who provided assistance with the handling of IGRF parameters. This study was supported by the IFREMER department of geosciences (DRO/GM).

References

Bear, G. W., H. J. Al-Shukri, and A. J. Rudman, Linear inversion of gravity data for 3-D density distributions, *Geophysics*, *60*, 1354–1364, 1995.

Bideau, D., R. Hékinian, B. Sichler, E. Gràcia, C. Bollinger, M. Constantin, and C. Guivel, Contrasting volcanic-tectonic process during the past 2 Ma on the Mid-Atlantic Ridge: Submersible mapping, petrological and magnetic results at lat. 34°52′N and 33°55′N, *Mar. Geophys. Res.*, *20*, 425–458, 1998.

Bonatti, E., and K. Crane, Oscillatory spreading explanation of anomalously old uplifted crust near oceanic transforms, *Nature*, *300*, 343–345, 1982.

Bonatti, E., and J. Honnorez, Nonspreading crustal blocks at the Mid-Atlantic Ridge, *Science*, *174*, 1329–1331, 1971.

Bonatti, E., J. R. Lawrence, and N. Morandi, Serpentinization of oceanic peridotites: Temperature dependence of mineralogy and boron content, *Earth Planet. Sci. Lett.*, *70*, 88–94, 1984.

Bonatti, E., M. Ligi, A. M. Borsetti, L. Gasperini, A. Negri, and R. Sartori, Lower Cretaceous deposits trapped near the equatorial Mid-Atlantic Ridge, *Nature*, *380*, 518–520, 1996.

Camacho, A. G., F. G. Montesinos, and R. Vieira, A three-dimensional gravity inversion applied to São Miguel Island (Azores), *J. Geophys. Res.*, *102*, 7717–7730, 1997.

Cande, S. C., and D. V. Kent, Revised calibration of the geomagnetic polarity timescale for the Late Cretaceous and Cenozoic, *J. Geophys. Res.*, *100*, 6093–6095, 1995.

Cannat, M., Y. Lagabrielle, H. Bougault, J. Casey, N. de Coutures, L. Dmitriev, and Y. Fouquet, Ultramafic and gabbroic exposures at the Mid-Atlantic Ridge: Geological mapping in the 15°N region, *Tectonophysics*, *279*, 193–213, 1997.

DeMets, C., R. G. Gordon, D. F. Argus, and S. Stein, Current plate motions, *Geophys. J. Int.*, *101*, 425–478, 1990.

Dunlop, D. J., and M. Prevot, Magnetic properties and opaque mineralogy of drilled submarine intrusive rocks, *Geophys. J. R. Astron. Soc.*, *69*, 763–802, 1982.

Dyment, J., and J. Arkani-Hamed, Contribution of lithospheric remanent magnetization to satellite magnetic anomalies over the world's oceans, *J. Geophys. Res.*, *103*, 15,423–15,441, 1998.

Escartín, J., P. A. Cowie, R. C. Searle, S. Allerton, N. C. Mitchell, C. J. MacLeod, and A. P. Slootweg, Quantifying tectonic strain and magnetic accretion at a slow spreading ridge segment, Mid-Atlantic Ridge, 29°N, *J. Geophys. Res.*, *104*, 10,421–10,437, 1999.

Forbes, J. M., The equatorial electrojet, *Rev. Geophys.*, *19*, 469–504, 1981.

Fox, P. J., and D. G. Gallo, A tectonic model for ridge-transform-ridge plate boundaries: Implication for the structure of oceanic lithosphere, *Tectonophysics*, *104*, 205–242, 1984.

Fox, P. J., and N. D. Opdyke, Geology of the oceanic crust: Magnetic properties of oceanic rocks, *J. Geophys. Res.*, *78*, 5139–5154, 1973.

Hall, J. M., and A. Muzzatti, Delayed magnetization of the deeper kilometer of oceanic crust at Ocean Drilling Project Site 504, *J. Geophys. Res.*, *104*, 12,843–12,851, 1999.

Hamano, Y., M. M. Bina, and K. Krammer, Paleomagnetism of the serpentinized peridotite from ODP Hole 670A, *Proc. Ocean Drill. Program Sci. Results*, *106/109*, 257–262, 1990.

Harrison, C. G. A., Marine magnetic anomalies: The origin of the stripes, *Annu. Rev. Earth Planet. Sci.*, *15*, 505–543, 1987.

Hékinian, R., T. Juteau, B. Sichler, R. Apprioual, E. Gràcia, S. Sichel, and G. Udintsev, Submersible exploration of St. Peter and St. Paul's rocks massif and the intra transform spreading centers of the equatorial Atlantic (abstract), *Eos Trans. AGU*, *79*(45), Fall Meet. Suppl., F856, 1998.

Hékinian, R., T. Juteau, E. Gracia, B. Sichler, S. Sichel, G. Udintsev, R. Apprioual, and M. Ligi, Submersible observations of equatorial Atlantic mantle: The St. Paul Fracture Zone region, *Mar. Geophys. Res.*, *21*, 529–560, 2000.

Johnson, H. P., and J. E. Pariso, Variations in oceanic crustal magnetization: Systematic changes in the last 160 million years, *J. Geophys. Res.*, *98*, 435–445, 1993.

Katzman, R., U. S. ten Brink, and J. Lin, Three-dimensional modeling of pull-apart basins: Implications for the tectonics of the Dead Sea Basin, *J. Geophys. Res.*, *100*, 6295–6312, 1995.

Kelso, P. R., C. Richter, and J. E. Pariso, Rock magnetic properties, magnetic mineralogy, and paleomagnetism of peridotites from site 895, Hess Deep, *Proc. Ocean Drill. Program Sci. Results*, *147*, 405–413, 1996.

Kepezhinskas, P. K., Mantle anomalies and non-spreading lithospheric blocks in the Doldrums fracture zone, central Atlantic, *Mem. Soc. Geol. Ital.*, *44*, 243–258, 1990.

Kinoshita, H., T. Furata, and J. Pariso, Downhole magnetic field measurements and paleomagnetism, Hole 504B, Costa Rica Ridge, *Proc. Ocean Drill. Program Sci. Results*, *111*, 147–156, 1989.

Lagabrielle, Y., D. Bideau, M. Cannat, J. A. Karson, and C. Mével, Ultramafic-mafic plutonic rock suites exposed along the Mid-Atlantic Ridge (10°N–30°N): Symmetrical-asymmetrical distribution and implications for seafloor spreading processes, in *Faulting and Magmatism at Mid-Ocean Ridges*, *Geophys. Monogr. Ser.*, vol. 106, edited by W. R. Buck et al., pp. 153–176, AGU, Washington, D. C., 1998.

Lawrence, R. M., J. S. Gee, and S. D. Hurst, Magnetic anisotropy in serpentinized peridotites from site 920: Its origin and relationship to deformation fabrics, *Proc. Ocean Drill. Program Sci. Results*, *153*, 419–426, 1997.

Le Quentrec, M.-F., and B. Sichler, 3D inversion of deep tow magnetic data on the Atlantis II Deep (Red Sea): Hydrothermal and geodynamic interpretation, *Tectonophysics*, *198*, 421–439, 1991.

Lienert, B. R., and P. J. Wasilewski, A magnetic study of the serpentinization process at Burro Mountain, California, *Earth Planet. Sci. Lett.*, *43*, 406–416, 1979.

Lonsdale, P., Segmentation of the Pacific-Nazca spreading center, 1°N–20°S, *J. Geophys. Res.*, *94*, 12,197–12,225, 1989.

Menke, W., *Geophysical Data Analysis: Discrete Inverse Theory*, 260 pp., Academic, San Diego, Calif., 1984.

Nazarova, K. A., Serpentinized peridotites as a possible source for oceanic anomalies, *Mar. Geophys. Res.*, *16*, 455–462, 1994.

Onwumechili, C. A., Geomagnetic variations in the equatorial zone, in *Physics of Geomagnetic Phenomena*, edited by S. Matsuhita and W. H. Campbell, pp. 425–507, Academic, San Diego, Calif., 1967.

Opdyke, N. D., and R. Hékinian, Magnetic properties of some igneous rocks from the Mid-Atlantic Ridge, *J. Geophys. Res.*, *67*, 2257–2260, 1972.

Oufi, O., Les propriétés magnétiques des péridotites serpentinisées abyssales: Relation entre la composition chimique, la nature minéralogique des minéraux serpentineux et le comportement magnétique des péridotites serpentinisées, Ph.D. thesis, 277 pp., Univ. of Paris VII-Denis Diderot Univ., France, 2000.

Pariso, J. E., and H. P. Johnson, Magnetic properties and oxides petrography of the sheeted dikes complex in Hole 504B, *Proc. Ocean Drill. Program Sci. Results*, *111*, 159–167, 1989.

Pariso, J. E., and H. P. Johnson, Do layer 3 rocks make a significant contribution to marine magnetic anomalies? In situ magnetization of gabbros at Ocean Drilling Program Hole 735B, *J. Geophys. Res.*, *98*, 16,033–16,052, 1993.

Pariso, J. E., L. Stokking, and S. Allerton, Rock magnetism and magnetic mineralogy of a 1-km section of structural dikes, Hole 504B, *Proc. Ocean Drill. Program Sci. Results*, *137/140*, 253–262, 1995.

Pariso, J. E., C. Rommevaux, and J.-C. Sempere, Three-dimensional inversion of marine magnetic anomalies: Implications for crustal accretion along the Mid-Atlantic Ridge (28°–31°30′N), *Mar. Geophys. Res.*, *18*, 85–101, 1996.

Parker, R. L., and S. P. Huestis, The inversion of magnetic anomalies in the presence of topography, *J. Geophys. Res.*, *79*, 1587–1593, 1974.

Peyve, A., et al., New data on some major MAR structures: Preliminary results of R/V *Akademic Nicolaj Strakhov* 22 cruise, *InterRidge News*, *9*, 28, 2000.

Pockalny, R. A., A. Smith, and P. Gente, Spatial temporal variability of crustal magnetization of a slowly spreading ridge: Mid-Atlantic Ridge (20°–24°N), *Mar. Geophys. Res.*, *17*, 301–320, 1995.

Purucker, M. E., and J. Dyment, Satellite magnetic anomalies related to seafloor spreading in the South Atlantic Ocean, *Geophys. Res. Lett.*, *27*, 2765–2768, 2000.

Riddihough, R. P., Diurnal corrections to magnetic surveys: An assessment of errors, *Geophys. Prospect.*, *19*, 551–567, 1971.

Roeser, H. A., and H.-O. Bargeloh, Reduction of geomagnetic measurements at sea in the vicinity of the geomagnetic equator, *Dtsch. Hydrogr. Z.*, *41*, 237–255, 1988.

Rohr, K. M. M., The valley that time forgot, *Nature*, *380*, 480–481, 1996.

Ruegg, J.-C., M. Kasser, and J.-C. Lépine, Strain accumulation across the Asal-Ghoubbet rift, Djibouti, East Africa, *J. Geophys Res.*, *89*, 6237–6246, 1984.

Rusby, R. I., Segmentation and reorganization of the equatorial Mid-Atlantic (5°–0°N), *Bridge News*, *16*, 19, 1993.

Sandwell, D. T., and W. H. F. Smith, Marine gravity anomaly from Geosat and ERS 1 satellite altimetry, *J. Geophys Res.*, *102*, 10,039–10,054, 1997.

Schilling, J.-G., B. B. Hanan, B. McCully, R. H. Kingsley, and D. Fontignie, Influence of the Sierra Leone mantle plume on the equatorial Mid-Atlantic Ridge: A Nd-Sr-Pb isotopic study, *J. Geophys. Res.*, *99*, 12,005–12,028, 1994.

Sempéré, J. C., L. Kristjansson, H. Schouten, J. R. Heirtzler, and G. L. Johnson, A detailed study of the Reykjanes Ridge between 63°00′N and 63°40′N, *Mar. Geophys. Res.*, *12*, 215–234, 1990.

Shu-Kun, H., XCORR: A cross-over technique to adjust track data, *Comput. Geosci.*, *21*, 259–271, 1995.

Sichler, B., G. A. Auffret, D. Bideau, and R. Hékinian, 3D inversion of magnetic data collected in five areas of the Mid-Atlantic Ridge axis between Azores and equator, paper presented at the XI Meeting, Eur. Union of Geosci., Strasbourg, France, April 2001.

Smith, G. M., and S. K. Banerjee, Magnetic structure of the upper kilometer of the marine crust at Deep Sea Drilling Project Hole 504B, eastern Pacific Ocean, *J. Geophys. Res.*, *91*, 10,337–10,354, 1986.

Smith, W. H. F., and D. T. Sandwell, Bathymetric prediction from dense satellite altimetry and sparse shipboard bathymetry, *J. Geophys. Res.*, *99*, 21,803–21,824, 1994.

Stokking, L. B., E. A. Heise, S. Allerton, and H.-U. Worm, Data report: Magnetic properties and magnetic oxide mineralogy of upper crustal rocks from Holes 504B and 896A, *Proc. Ocean Drill. Program Sci. Results*, *148*, 467–482, 1996.

Strykowski, G., Geodetic and geophysical inverse gravimetric problem, the most adequate solution and the information content, in *Gravity and Geoid: Joint Symposium of the International Gravity Commission and the International Geoid Commission, Graz, Austria, September 11-17, 1994*, edited by H. Sünkel and I. Marson, pp. 215–224, Springer-Verlag, New York, 1995.

Talwani, M., Computation with help of a digital computer of magnetic anomalies caused by bodies of arbitrary shape, *Geophysics*, *30*, 797–817, 1965.

Tarantola, A., *Inverse Problem Theory Methods for Data Fitting and Model Parameter Estimation*, 613 pp., Elsevier Sci., New York, 1987.

Tarantola, A., and B. Valette, Inverse problems: Quest for information, *J. Geophys.*, *50*, 159–170, 1982.

Tarantola, A., J.-C. Ruegg, and J.-C. Lépine, Geodetic evidence for rifting in Afar: A brittle-elastic model of the behaviour of the lithosphere, *Earth Planet. Sci. Lett.*, *45*, 435–444, 1979.

Tivey, M. A., Fine-scale magnetic anomaly field over the southern Juan de Fuca Ridge: Axial magnetization low and implications for crustal structure, *J. Geophys. Res.*, *99*, 4833–4855, 1994.

Tivey, M. A., Vertical magnetic structure of ocean crust determined from near-bottom magnetic field measurements, *J. Geophys. Res.*, *101*, 20,275–20,296, 1996.

Tivey, M. A, and B. E. Tucholke, Magnetization of 0–29 Ma ocean crust on the Mid-Atlantic Ridge, 25°30′ to 27°10′N, *J. Geophys. Res.*, *103*, 17,807–17,826, 1998.

Tucholke, B. E., and J. Lin, A geological model for the structure of ridge segments in slow spreading ocean crust, *J. Geophys. Res.*, *99*, 11,937–11,958, 1994.

Tucholke, B. E., J. Lin, and M. C. Kleinrock, Megamullion and mullion structure defining oceanic metamorphic ore complexes on the Mid-Atlantic Ridge, *J. Geophys. Res.*, *103*, 9857–9866, 1998.

Udintsev, G. B., N. A. Kurentsova, N. V. Pronina, S. B. Smirnova, and M. G. Ushakova, Finds of continental rocks and sediments of anomalous age in the equatorial segment of the Mid-Atlantic Ridge, *Trans. USSR Acad. Sci., Dokl.*, *312*, 111–114, 1990.

Vine, F. H., and D. H. Matthews, Magnetic anomalies over oceanic ridges, *Nature*, *199*, 947–949, 1963.

R. Hékinian and B. Sichler, Institut Français de Recherche pour l'Exploitation de la Mer DRO/GM, Centre de Brest, BP 70, F-29280 Plouzané, France. (hékinian@ifremer.fr; bsichler@ifremer.fr)